Design of Impact-Free Gaits for Planar Bipeds and Their Stabilization Using Impulsive Control

Aakash Khandelwal[®], Nilay Kant[®], and Ranjan Mukherjee[®], Senior Member, IEEE

Abstract—The problem of designing and stabilizing impact-free gaits is considered for point-foot planar bipeds. A set of geometric constraints, which eliminate impact forces at the time of leg interchange, are used to design the gaits. A family of gaits, where the stride length and walking speed can be chosen independently for each gait, is guaranteed to exist. A continuous controller is used to enforce the constraints associated with a desired gait and intermittent impulsive inputs are applied to stabilize the gait. A five-link biped example is used to illustrate the procedure for designing impact-free gaits. The effectiveness of the continuous and impulsive controllers, working in tandem for stabilization of a gait, is shown using simulations.

Index Terms—Humanoid and bipedal locomotion, motion control, underactuated robots.

I. INTRODUCTION

OINT-FOOT bipeds represent a class of underactuated hybrid dynamical systems; the hybrid nature can be attributed to the impulsive dynamics at the time of swing leg touchdown and coordinate resetting associated with the interchange of stance and swing legs. For bipedal locomotion, an important problem is to design and stabilize a gait, which is a periodic hybrid orbit. Virtual Holonomic Constraints (VHCs) [1], [2], [3], [4] have been used to design biped gaits [5], [6], [7], [8], [9], [10], [11], [12]; a set of geometric constraints are imposed on the joint variables to eliminate the need for tracking time-varying reference trajectories for each joint. The VHCs are typically enforced using feedback and the biped trajectories are confined to lie on a constraint manifold during the swing phase. The VHCs must additionally ensure hybrid invariance of the constraint manifold; this implies that a nominal gait evolving on the constraint manifold during the swing phase must return to the constraint manifold after jump in velocities due to foot-ground interaction and coordinate

In the well-known works on bipedal locomotion by Grizzle and collaborators, [5], [6], [7], for example, the VHCs are parametrized using Bézier polynomials. To enforce the VHCs, a nonsmooth controller is used for finite-time convergence of the trajectories to the constraint manifold in the swing phase after every step. Under the assumption of finite-time convergence, the gait is described by a reduced-order Poincaré map; the conditions for existence and asymptotic stability of the gait are a set of inequality constraints [13]. Subject to these constraints, and additional constraints such as the walking speed, an asymp-

Manuscript received 17 May 2023; accepted 29 August 2023. Date of publication 11 September 2023; date of current version 27 September 2023. This letter was recommended for publication by Associate Editor K. Akbari Hamed and Editor A. Kheddar upon evaluation of the reviewers' comments. This work was supported by the National Science Foundation, under Grant CMMI-2043464. (Corresponding author: Ranjan Mukherjee.)

The authors are with the Department of Mechanical Engineering, Michigan State University, East Lansing, MI 48824 USA (e-mail: khande 10@egr.msu.edu; kantnila@egr.msu.edu; mukherji@egr.msu.edu).

This letter has supplementary downloadable material available at $\frac{1}{100}$ https://doi.org/10.1109/LRA.2023.3313940, provided by the authors.

Digital Object Identifier 10.1109/LRA.2023.3313940

totically stable biped gait is sought through numerical optimization. Although this approach has been validated in three [12] and five [5], [6], [8] DOF bipeds, the existence of an asymptotically stable gait cannot be guaranteed for the general case as it is based on numerical optimization. The assumption of finite-time convergence necessitates controller tuning based on stride length and walking speed. If desired gait characteristics such as the walking speed are changed, the optimization has to be repeated. The numerical optimization is computationally expensive for high-DOF bipeds, although a less expensive algorithm was recently proposed [9]. Freidovich et al., [10] replaced the nonsmooth controller in [12] with a smooth approximation and studied gait stability using transverse linearization for a three-DOF biped. Note that the VHC was not enforced in this approach and its applicability to high-DOF bipeds is unclear. In an alternate approach, VHCs were enforced using a smooth controller [14] designed via control Lyapunov functions. The VHC-based gait designs in [9], [10], [14] are, in essence, variations of the optimization-based approach by Grizzle [7] wherein the existence of an asymptotically stable gait cannot be guaranteed a

We adopt a fundamentally different approach to design and stabilization of gaits for general point-foot planar bipeds. Using VHCs, we design gaits which are impact-free, i.e., no impulsive forces are applied by the ground on the swing foot at the time of touch down. The VHCs are enforced using a continuous controller and a desired gait is stabilized using impulsive control inputs applied intermittently on a Poincaré section. Contrary to the perception that impulsive inputs are a theoretical construct and are impractical, continuous-time approximations of impulsive inputs have been experimentally demonstrated in the control of underactuated systems using standard hardware [15], [16], [17], [18]. The results presented here are validated using simulations but can be suitably implemented in a standard biped. In relation to prior works, the novelty of our approach is as follows:

- The gait parameters are determined by solving a set of algebraic equations, and existence of a family of gaits is guaranteed.
- The gait parameters can be computed for a desired stride length and the speed of walking can be arbitrarily chosen for a given set of gait parameters.
- Since the gait is impact-free, hybrid invariance can be ensured using algebraic relations related to coordinate resetting alone.
- The use of impulsive inputs allows us to treat gait design and gait stabilization as two independent problems.
- The use of impulsive inputs eliminates reliance on foot-ground impact forces for gait stabilization. The stabilizability of the gait can be checked analytically and the rate of convergence to the desired gait can be tuned.
- The computational cost of gait design does not scale adversely with DOF.
- The VHCs can be enforced using a smooth controller and finitetime convergence of the trajectories to the constraint manifold is not required.
- Since the nominal gait is impact-free, our approach to gait design and stabilization minimizes impulsive forces due to foot-ground interaction; this has the potential to reduce wear and tear, unwanted vibrations, energy loss, and sensor noise.

2377-3766 © 2023 IEEE. Personal use is permitted, but republication/redistribution requires IEEE permission. See https://www.ieee.org/publications/rights/index.html for more information.

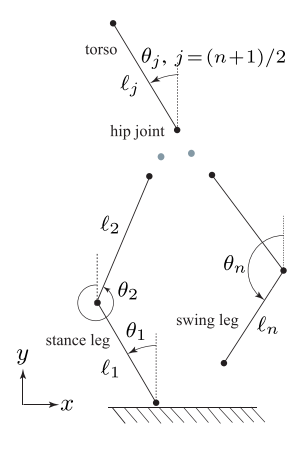


Fig. 1. *n*-link point-foot planar biped.

II. SYSTEM DYNAMICS

A. System Description and Assumptions

Consider the n-link planar biped (n is odd) comprised of a single-link torso and kinematically similar legs with point feet - see Fig. 1. It is assumed that the biped gait is comprised of a sequence of steps, where each step is comprised of a single-support phase (one leg is in contact with the ground) and a double-support phase (both legs are in contact with the ground). In the single-support phase, the leg in contact with the ground is referred to as the stance leg and the other leg is referred to as the swing leg. The stance foot is passive; it does not slide or leave the ground and acts as a frictionless pivot. The single-support phase ends when the swing leg comes in contact with the ground. The ensuing double-support phase is of infinitesimal duration; during this phase, there is force interaction between the ground and the swing leg but not between the ground and the stance leg. The double-support phase ends with relabelling of coordinates for interchange of the stance and swing legs.

Each leg has (n-1)/2 links; the stance leg links are numbered sequentially 1 through (n-1)/2 starting from the link in contact with the ground, the torso is link (n+1)/2, and the swing leg links are numbered sequentially (n+3)/2 through n starting from the link in contact with the torso. The length of the j-th link, $j=1,2,\ldots,n$, is ℓ_j . Since the legs are kinematically identical, the link lengths satisfy

$$\ell_{n-j+1} = \ell_j \quad \forall j = 1, 2, \dots, (n-1)/2$$

The center-of-mass of the j-th link is located at a distance d_j from joint j. The mass and mass moment of inertia about the center-of-mass of the j-th link are denoted by m_j and J_j . The orientation of the j-th link, $j=1,2,\ldots,n$, measured counter-clockwise with respect to the vertical, is denoted by θ_j . The link $j,j=2,\ldots,n$, is driven by an actuator mounted on link (j-1), which applies torque τ_j .

The dynamics of the biped in the single-support phase, also known as the swing phase, is discussed in Section II-B. The dynamics of footground interaction and the relabelling of coordinates for interchange of the stance and swing legs in the double-support phase is discussed in Section II-C. For generality and ease of control design, the dynamics are presented using the generalized coordinates $q \triangleq \begin{bmatrix} q_1^T \mid q_2 \end{bmatrix}^T$, where $q_1 \in \mathcal{Q}^{n-1}, \ q_2 \in \mathcal{Q}^1$ and $\mathcal{Q}^n \triangleq S^1 \times S^1 \times \cdots \times S^1$. We define the generalized coordinates q as follows

$$q = \begin{bmatrix} (\theta_2 - \theta_1) & (\theta_3 - \theta_2) & \cdots & (\theta_n - \theta_{n-1}) & \theta_1 \end{bmatrix}^T - \Pi$$
 (1)

where $\Pi \in \mathbb{R}^n$ has elements equal to zero for all entries except for the (n+1)/2 entry, which is equal to π .

B. Swing Phase Dynamics: Continuous and Impulsive Inputs

During the swing phase, the biped represents an n-DOF underactuated system with one passive DOF q_2 . The kinetic and potential energies of the system are denoted by $T(q,\dot{q})=\frac{1}{2}\dot{q}^TM(q)\dot{q}$ and V(q) respectively, where $M\in R^{n\times n}$ is the symmetric, positive definite mass matrix:

$$M(q) = \begin{bmatrix} M_{11}(q) & M_{12}(q) \\ M_{12}^{T}(q) & M_{22}(q) \end{bmatrix}$$

where $M_{11} \in R^{(n-1)\times(n-1)}$, $M_{22} \in R$ and the equations of motion can be written in the same form as in [3]:

$$M_{11}(q)\ddot{q}_1 + M_{12}(q)\ddot{q}_2 + h_1(q,\dot{q}) = u$$
 (2a)

$$M_{12}^T(q)\ddot{q}_1 + M_{22}(q)\ddot{q}_2 + h_2(q,\dot{q}) = 0$$
 (2b)

where $\begin{bmatrix} h_1^T & h_2 \end{bmatrix}^T \in R^n$ is the vector of Coriolis, centrifugal, and gravity forces, and $u \triangleq \begin{bmatrix} \tau_2 & \tau_3 & \cdots & \tau_n \end{bmatrix}^T \in R^{n-1}$ is the control input vector. The equation can be rewritten as:

$$\ddot{q}_1 = A(q, \dot{q}) + B(q)u, \quad \ddot{q}_2 = C(q, \dot{q}) + D(q)u$$
 (3)

where the expressions for $A(q,\dot{q})$, B(q), $C(q,\dot{q})$ and D(q) can be found in [3]. Since the biped has revolute joints, we make the following assumption [2], [3].

Assumption 1: For the n-link biped, the mass matrix and the potential energy are even functions of q:

$$M(q) = M(-q), \quad V(q) = V(-q)$$

When u is continuous and has the form $u=u_c(q,\dot{q})$, the dynamics in (2) has the state-space representation

$$\dot{x} = f(x), \quad x \triangleq \begin{bmatrix} q^T & \dot{q}^T \end{bmatrix}^T \in \mathcal{Q}^n \times R^n$$
 (4)

If an impulsive input $u_{\mathcal{I}}$ is applied in addition to u_c at any instant, the system will experience a discontinuous change in the generalized velocities with no change in the generalized coordinates [19]. The jump in the generalized velocities can be obtained by integrating (2) as follows:

$$\begin{bmatrix} M_{11} & M_{12} \\ M_{12}^T & M_{22} \end{bmatrix} \begin{bmatrix} \Delta \dot{q}_1 \\ \Delta \dot{q}_2 \end{bmatrix} = \begin{bmatrix} \mathcal{I} \\ 0 \end{bmatrix}, \quad \mathcal{I} \triangleq \int_0^{\Delta t} u_{\mathcal{I}} dt$$
 (5)

where Δt is the infinitesimal duration for which $u_{\mathcal{I}}$ is active, $\mathcal{I} \in \mathbb{R}^{n-1}$ is the impulse of $u_{\mathcal{I}}$,

$$\Delta \dot{q}_1 \triangleq (\dot{q}_1^+ - \dot{q}_1^-), \quad \Delta \dot{q}_2 \triangleq (\dot{q}_2^+ - \dot{q}_2^-)$$

and $(.)^-$ and $(.)^+$ denote the variable (.) immediately before and after an event where there is a discontinuous jump in its value. The states immediately after application of the impulsive input can be expressed as

$$x^{+} = x^{-} + \Delta x_{\mathcal{I}}, \quad \Delta x_{\mathcal{I}} \triangleq \begin{bmatrix} 0 \\ \Delta \dot{q} \end{bmatrix}$$
 (6)

where $\Delta \dot{q}$ is obtained from (5).

Remark 1: In actuators such as motors, continuous-time approximation of an impulsive input $u_{\mathcal{I}}$ can be realized using high-gain feedback [15], [16], [17]. An expression for the high-gain feedback will be provided in Section IV-C.

Remark 2: Impulsive inputs have been extensively used in control of underactuated systems, see for instance [3], [15], [16], [17], [18], [20], [21], [22], [23] for theoretical and experimental results.

C. Foot-Ground Interaction and Coordinate Relabelling

In the double-support phase, there is impulsive interaction between the swing foot and the ground. The stance foot lifts from the ground without interaction, and there is an instantaneous interchange between stance and swing legs.

Following the approach in [12], [24], the impact between the swing foot and the ground is modeled as an inelastic collision. This model is

described using (n+2) DOF, which includes the original n DOFs and the two Cartesian coordinates of the stance foot (s_x, s_y) , $s_x, s_y \in R$. The equations of motion of the extended system can be written in the form

$$M_e(q_e)\ddot{q}_e + h_e(q_e, \dot{q}_e) = p_e + p^{\text{ext}}, \quad q_e \triangleq \left[q^T \quad s_x \quad s_y \right]^T$$
 (7)

where $M_e \in R^{(n+2)\times (n+2)}$ is the mass matrix, $h_e \in R^{n+2}$ is the vector of Coriolis, centrifugal, and gravity forces, $p_e = \begin{bmatrix} u^T & 0 & 0 & 0 \end{bmatrix}^T \in R^{n+2}$ is the vector of generalized forces, and $p^{\mathrm{ext}} \in R^{n+2}$ is the vector of generalized impulsive forces due to interaction between the swing foot and the ground. The discontinuous change in the generalized velocities due to p^{ext} can be obtained by integrating (7)

$$M_e(q_e) \, \Delta \dot{q}_e = \mathcal{I}^{\text{ext}}, \quad \mathcal{I}^{\text{ext}} \triangleq \int_0^{\Delta t} p^{\text{ext}} dt$$
 (8)

where Δt is the infinitesimal duration of the impact, $\mathcal{I}^{\mathrm{ext}} \in R^{n+2}$ is the impulse due to p^{ext} , and $\Delta \dot{q}_e \triangleq (\dot{q}_e^+ - \dot{q}_e^-)$. Let F_x and F_y denote the Cartesian components of the impulsive forces on the swing foot due to impact. Then

$$p^{\text{ext}} = \Gamma^T F, \quad \Gamma \triangleq \frac{\partial \gamma}{\partial q_e}, \quad \gamma \triangleq \begin{bmatrix} \gamma_x \\ \gamma_y \end{bmatrix}, \quad F \triangleq \begin{bmatrix} F_x \\ F_y \end{bmatrix}$$
 (9)

where $\gamma \equiv \gamma(q_e) \in R^2$ denotes the Cartesian coordinates of the swing foot. By integrating (9) over the duration of impact Δt , we get

$$\mathcal{I}^{\text{ext}} = \Gamma^T \mathcal{I}_{\text{g}}, \quad \mathcal{I}_{\text{g}} \triangleq \int_0^{\Delta t} F dt$$
 (10)

Since the foot-ground collision is inelastic,

$$\Gamma \dot{q}_e^+ = 0 \tag{11}$$

Using (8), (10) and (11), we get

$$\begin{bmatrix} M_e & -\Gamma^T \\ \Gamma & 0 \end{bmatrix} \begin{bmatrix} \dot{q}_e^+ \\ \mathcal{I}_g \end{bmatrix} = \begin{bmatrix} M_e \dot{q}_e^- \\ 0 \end{bmatrix}$$
 (12)

The states immediately after foot-ground interaction are

$$x^{+} = x^{-} + \Delta x_{\rm g}, \quad \Delta x_{\rm g} \triangleq \begin{bmatrix} 0 \\ \Delta \dot{q} \end{bmatrix}$$
 (13)

where $\Delta \dot{q}$ is obtained using (12).

The subsequent interchange of the stance and swing legs is equivalent to a relabelling of states [25]. The states immediately after leg interchange are a function of those immediately before interchange, and is given by the relation:

$$x^+ = \mathcal{R}(x^-)$$

$$\mathcal{R}(x) = \text{blockdiag} \begin{bmatrix} U & U \end{bmatrix} x - \begin{bmatrix} \Pi^T \mid 0_{1 \times n} \end{bmatrix}^T$$
 (14)

where $0_{i\times j}\in R^{i\times j}$ is the matrix of zeros and $U\in R^{n\times n}$ has elements given by $U_{ij}=-1$ for $i+j=n,\ U_{ij}=1$ for i=n, and $U_{ij}=0$ otherwise.

D. Hybrid Dynamic Model

The hybrid dynamics of the gait is described as follows

$$\mathcal{D}: \begin{cases} \dot{x} = f(x), & x \notin \mathcal{S}, u_{\mathcal{I}} = 0 & \text{(1)} \\ x^{+} = x^{-} + \Delta x_{\mathcal{I}}, & x^{-} \notin \mathcal{S}, u_{\mathcal{I}} \neq 0 & \text{(2)} \\ x^{+} = x^{-} + \Delta x_{g}, & x^{-} \in \mathcal{S}_{1} & \text{(3)} \\ x^{+} = \mathcal{R}(x^{-}), & x^{-} \in \mathcal{S}_{2} & \text{(4)} \end{cases}$$

where

$$S_1 \triangleq \{x \in \mathcal{Q}^n \times R^n : \gamma_y = 0, \dot{\gamma}_y < 0\}$$
 (16a)

$$S_2 \triangleq \{ x \in \mathcal{Q}^n \times R^n : \gamma_y = 0, \dot{\gamma} = 0 \}$$
 (16b)

and $\mathcal{S} \triangleq \mathcal{S}_1 \cup \mathcal{S}_2$ is the set of states during the double-support phase. The different components of the hybrid dynamics \mathcal{D} over a step are illustrated with the help of Fig. 2 for a single impulsive actuation during the swing phase.

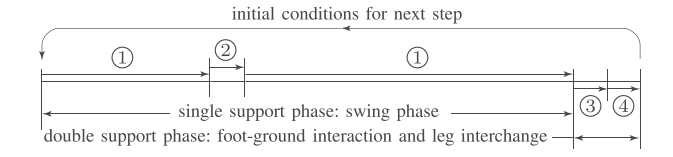


Fig. 2. Hybrid dynamics of biped over a step with a single impulsive actuation during the swing phase. The different components are: ①: continuous-time dynamics, ②: jump in states due to impulsive actuation, ③: jump in states due to foot-ground interaction, and ④: change of states due to coordinate relabelling.

III. IMPACT-FREE GAITS

For ease of gait design, we use the physical coordinates $\theta_1, \theta_2, \dots, \theta_n$. Once the design is completed, the gait is described by VHCs in the generalized coordinates q.

A. Boundary Conditions for Impact-Free Gaits

We use superscripts $(.)^i$ and $(.)^f$ to denote the value of (.) at the beginning and end of the swing phase, respectively. A gait will be impact-free if no impulsive forces are applied by the ground on the swing foot at the time of touch down. This requires the following conditions to be satisfied:

$$\dot{\gamma}^f = -\sum_{\substack{j=1\\j\neq(n+1)/2}}^n \ell_j \begin{bmatrix} \cos\theta_j^f\\ \sin\theta_j^f \end{bmatrix} \dot{\theta}_j^f = 0 \tag{17}$$

where link (n+1)/2 is the torso and hence excluded. To design the gait, we will impose additional boundary conditions [26] that ensure identical potential and kinetic energies at the beginning and end of the swing phase:

$$\theta_{i}^{f} = -\theta_{i}^{i}, \quad j = 1, 2, \dots, n$$
 (18)

$$\dot{\theta}_{j}^{f} = \dot{\theta}_{j}^{i}, \qquad j = 1, 2, \dots, n$$
 (19)

The boundary conditions in (18) are the simplest relations that satisfy the potential energy condition. The conditions in (17), (18) and (19) will be satisfied through the design of actuated joint trajectories, presented next.

B. Gait Design

We begin the gait design by choosing $\theta_1^f=-\theta_1^i$. We then design the actuated joint trajectories as follows:

$$\theta_i = a_i \theta_1 + k_i \pi + f_i^o(\theta_1), \quad j = 2, 3, \dots, n$$
 (20)

where $a_j \in R$ and $k_j \in \{0,1\}$ are constants, and $f_j^o(\theta_1)$ is an odd function. The above design ensures that (18) is satisfied for all actuated joint angles.¹

Taking the time derivative of (20), we obtain

$$\dot{\theta}_j = \left[a_j + \frac{df_j^o}{d\theta_1} \right] \dot{\theta}_1, \quad j = 2, 3, \dots, n$$
 (21)

In the above equation, $[a_j + (df_j^o/d\theta_1)]$ is an even function of θ_1 ; therefore (19) will be satisfied if $\dot{\theta}_1$ is an even function of θ_1 . We will show in Section III-D that this requirement can be satisfied for the trajectories in (20).

C. Boundary Conditions on Joint Trajectories

For a single-step periodic gait, the configurations at the beginning and end of the swing phase are symmetric about the vertical passing

¹Since θ_j is a revolute joint angle, the boundary conditions physically remain unchanged if we subtract 2π when $k_j=1$, effectively changing the term $+\pi$ to $-\pi$

through the stance foot, i.e.,

$$\theta_{n-j+1}^f = \theta_j^i - \pi \quad \forall j = 1, 2, \dots, (n-1)/2$$
 (22a)

$$\theta_j^f = \theta_j^i \qquad j = (n+1)/2 \tag{22b}$$

Using (18), we get

$$\theta_{n-j+1}^i = -\theta_j^i + \pi \quad \forall j = 1, 2, \dots, (n-1)/2$$
 (23a)

$$\theta^i_j=-\theta^i_j \qquad j=(n+1)/2 \tag{23b}$$
 From (23b), it follows
$$\theta^i_j=0 \quad j=(n+1)/2 \tag{24}$$

$$\theta_i^i = 0 \quad j = (n+1)/2 \tag{24}$$

The joint velocities must satisfy

$$\dot{\theta}_{n-j+1}^f = \dot{\theta}_j^i \quad \forall j = 1, 2, \dots, (n-1)/2$$
 (25)

$$\dot{\hat{\theta}}_{n-j+1}^i = \dot{\theta}_j^i \quad \forall j = 1, 2, \dots, (n-1)/2$$
 (26)

By substituting (18) and (19) in (17), we obtain

$$\sum_{\substack{j=1\\j\neq(n+1)/2}}^{n} \ell_{j} \begin{bmatrix} \cos\theta_{j}^{i}\\ -\sin\theta_{j}^{i} \end{bmatrix} \dot{\theta}_{j}^{i} = 0 \tag{27}$$

Since the legs are kinematically identical, substitution of (23) and (26) into (27) yields

$$\sum_{i=1}^{(n-1)/2} \ell_j \sin \theta_j^i \, \dot{\theta}_j^i = 0 \tag{28}$$

and the first equation in (27) is trivially satisfied.

Remark 3: It follows from (21) that the conditions in (26) and (28) are independent of the value of $\dot{\theta}_1^i$. Thus, the n+1 conditions in (23a), (24), (26) and (28) depend only on the choice of θ_1^i .

In the Appendix, we present a constructive proof that impact-free gaits can always be designed for n > 5.

D. VHCs for Impact-Free Gait

To proceed with the control design for gait stabilization, the joint trajectories in (20), subject to the conditions in (23a), (24), (26) and (28), are expressed as VHCs in terms of the generalized coordinates q, using (1) as follows:

$$\rho(q) = q_1 - \Phi(q_2) = 0, \quad \Phi: S^1 \to \mathcal{Q}^{n-1}$$
(29)

The corresponding constraint manifold C is given by:

$$C = \left\{ (q, \dot{q}) : q_1 = \Phi(q_2), \dot{q}_1 = \left[\frac{\partial \Phi}{\partial q_2} \right] \dot{q}_2 \right\}$$
 (30)

Remark 4: For the choice of generalized coordinates in (1), the approach in the Appendix ensures that the VHCs in (29) are odd, i.e., $\Phi(q_2) = -\Phi(-q_2)$ [3, Assumption 2].

Remark 5: The VHCs in (29) are regular and C is stabilizable if $M_{12}^T(\partial \Phi/\partial q_2) + M_{22} \neq 0$ [3, Remark 1].

The continuous control u_c in [3]:

$$u_c = [B - (\partial \Phi / \partial q_2)D]^{-1} \left[-A + (\partial^2 \Phi / \partial q_2^2) \dot{q}_2^2 + (\partial \Phi / \partial q_2)C - k_p \rho - k_d \dot{\rho} \right]$$
(31)

where k_p and k_d are positive definite matrices, drives $\rho(t)$ to zero exponentially, enforcing the VHC in (29) and rendering ${\cal C}$ controlled invariant.

By substituting (29) in (2b), we get the swing phase zero dynamics [3], [27]:

$$\ddot{q}_2 = \alpha_1(q_2) + \alpha_2(q_2)\dot{q}_2^2 \tag{32}$$

The zero dynamics in (32) has an integral of motion $E(q_2, \dot{q}_2)$ [1], [2], and its qualitative properties can be described by a potential energy function $\mathcal{P}(q_2)$, which has minimum and maximum values \mathcal{P}_{\min} and \mathcal{P}_{max} [2]. For energy level sets $E(q_2, \dot{q}_2) = c$, a feasible biped gait corresponds to one for which $c > \mathcal{P}_{\max}$, which ensures that q_2 is an even function of q_2 and does not change sign during the swing phase;

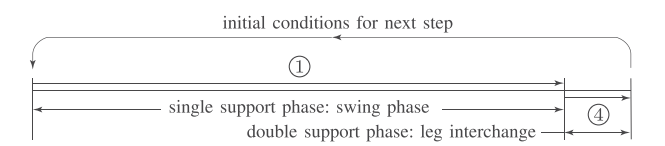


Fig. 3. Hybrid dynamics of biped over a step for an impact-free gait; it is a simpler version of the dynamics shown in Fig. 2 with components: (1): continuous-time dynamics, (4): change of states due to coordinate relabelling.

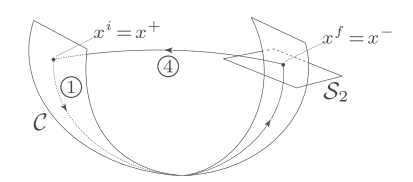


Fig. 4. Evolution of system trajectory during an impact-free gait.

thus the biped is able to complete a step. This will be accomplished through proper choice of initial conditions.

A system trajectory in C satisfies $\dot{\gamma}^f = 0 \ \forall x \in C$. Thus, $C \cap S_1 = \emptyset$ and consequently $\mathcal{C} \cap \mathcal{S} = \mathcal{C} \cap \mathcal{S}_2$. A trajectory evolving in \mathcal{C} in the single-support phase will intersect S_2 in the double-support phase. This results in a discontinuous jump in states described by (14). Although the trajectory may leave C during the jump, it can be shown that the new states lie in C, i.e., C is invariant under relabelling of the states:

$$\mathcal{R}(\mathcal{C} \cap \mathcal{S}_2) \subset \mathcal{C} \tag{33}$$

The components of the hybrid dynamics over a step for an impact-free gait are shown in Fig. 3; the evolution of the system trajectory is shown in Fig. 4.

IV. STABILIZATION OF AN IMPACT-FREE GAIT

A. Orbit Describing an Impact-Free Gait

An impact-free gait, described by the VHCs in (29), is the hybrid orbit:

$$\mathcal{O}^* = \mathcal{C}^* \cup \mathcal{R}^* \tag{34}$$

where

$$C^* = \{x \in C : E(q_2, \dot{q}_2) = c^*\} \qquad c^* > \mathcal{P}_{\text{max}}$$
 (35a)

$$\mathcal{R}^* = \{ x^-, x^+ : x^- \in \mathcal{C}^* \cap \mathcal{S}_2, x^+ = \mathcal{R}(x^-) \in \mathcal{C}^* \}$$
 (35b)

The orbit \mathcal{O}^* is stabilized using the ICPM approach [3], whose efficacy has been demonstrated for both continuous and hybrid orbits [3], [23].

B. Poincaré Map

To stabilize \mathcal{O}^* from any point in its neighborhood, we describe the hybrid dynamics in (15) using a discrete-time map. To this end, we define the Poincaré section:

$$\Sigma = \{ x \in \mathcal{Q}^n \times R^n : q_2 = q_2^*, \dot{q}_2 < 0 \}$$
 (36)

The states on Σ are:

$$z = \begin{bmatrix} q_1^T & \dot{q}^T \end{bmatrix}^T, \quad z \in \mathcal{Q}^{n-1} \times R^n$$
 (37)

We assume that impulsive actuation is applied when the system trajectory intersects Σ^2 . If z(k) denotes the states immediately prior to application of \mathcal{I} , the hybrid dynamics of the impulse-controlled system can be expressed as

$$z(k+1) = \mathbb{P}[z(k), \mathcal{I}(k)] \tag{38}$$

²It must be verified that \mathcal{O}^* and its perturbations are transversal to Σ [7].

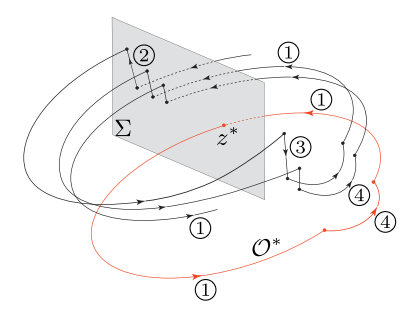


Fig. 5. Schematic of the ICPM approach to orbital stabilization of an impactfree gait. The desired orbit is shown in red. The different components of the hybrid dynamics, namely, (1), (2), (3) and (4) are described by (15).

The map \mathbb{P} captures the dynamics between subsequent intersections of the system trajectory with Σ . It is comprised of the components (2), (1), (3), (4), and (1), described in (15) and depicted in Fig. 2.

C. Orbital Stabilization

If $x \in \mathcal{O}^*$, the system trajectory is restricted to \mathcal{O}^* under continuous control u_c . The intersection of \mathcal{O}^* with Σ is therefore a fixed point $z(k) = z^*$, $\mathcal{I}(k) = 0$ of \mathbb{P}

$$z^* = \mathbb{P}(z^*, 0) \tag{39}$$

If $x \notin \mathcal{O}^*$, u_c does not guarantee convergence of the trajectory to \mathcal{O}^* , and the impulsive inputs $\mathcal{I}(k)$ are used to asymptotically stabilize the fixed point z^* , and consequently the orbit \mathcal{O}^* [3], [28]. To this end, we linearize the map \mathbb{P} about $z(k)=z^*$ and $\mathcal{I}(k)=0$ as follows:

$$e(k+1) = \mathcal{A}e(k) + \mathcal{B}\mathcal{I}(k), \quad e(k) \triangleq z(k) - z^*$$
 (40)

$$\mathcal{A} \triangleq [\nabla_z \mathbb{P}(z, \mathcal{I})]_{z=z^*, \mathcal{I}=0}$$

$$\mathcal{B} \triangleq \left[\nabla_{\mathcal{I}} \mathbb{P}(z, \mathcal{I}) \right]_{z = z^* \ \mathcal{I} = 0} \tag{41}$$

The matrices $\mathcal{A} \in R^{(2n-1)\times(2n-1)}$ and $\mathcal{B} \in R^{(2n-1)\times(n-1)}$ can be computed numerically. If $(\mathcal{A},\mathcal{B})$ is controllable, the orbit \mathcal{O}^* can be stabilized by the discrete feedback:

$$\mathcal{I}(k) = \mathcal{K}e(k) \tag{42}$$

where $\mathcal K$ is chosen such that the eigenvalues of $(\mathcal A + \mathcal B \mathcal K)$ lie inside the unit circle.

The stabilization of \mathcal{O}^* using the ICPM approach [3], [23] is explained with the help of Fig. 5. The desired orbit \mathcal{O}^* (shown in red), intersects Σ at the fixed point z^* ; it corresponds to an impact-free gait where the states undergo a single discontinuous jump due to coordinate relabelling - see Fig. 4. For a trajectory not on \mathcal{O}^* (shown in black), there is a discontinuous jump in states ② on Σ due to application of $\mathcal{I}(k)$. A second discontinuous jump ③ occurs at the time of foot-ground interaction; this is immediately followed by the discontinuous jump ④ due to coordinate relabelling. The input $\mathcal{I}(k)$ in (42) guarantees asymptotic convergence of a system trajectory to \mathcal{O}^* . As the system trajectory converges to \mathcal{O}^* , the discontinuous jumps ② and ③ converge to zero.

Remark 6: The following high-gain feedback, applied in addition to u_c , can be used to realize a continuous-time approximation of impulsive inputs [3]:

$$u_{\rm hg} = B^{-1} \left[\frac{1}{\mu} \Lambda(\dot{q}_1^{\rm des}(k) - \dot{q}_1) - \bar{A} \right]$$
 (43)

where $\dot{q}_1^{\mathrm{des}}(k)=\dot{q}_1(k)+B\mathcal{K}e(k),\ \bar{A}=(1/M_{22})B(q)\times\ [M_{12}h_2-(h_1-u_c)M_{22}],\ \Lambda=\mathrm{diag}[\lambda_1\ \lambda_2\ \cdots\ \lambda_{n-1}],\ \lambda_i>0,\ i=1,2,\ldots,n-1,\ \mathrm{and}\ \mu>0$ is a small number. The high-gain feedback remains active as long as $\|\dot{q}_1^{\mathrm{des}}(k)-\dot{q}_1\|\geq\epsilon$ where ϵ is a small, positive number

TABLE I Kinematic and Dynamic Parameters of Five-Link Biped

j	ℓ_j (m)	d_j (m)	m_j (kg)	J_j (kg m 2)
1, 5	0.5000	0.2500	0.4000	0.0083
2, 4	0.5500	0.2750	0.4500	0.0113
3 (torso)	0.6000	0.4200	0.5500	0.0165

TABLE II IMPACT-FREE GAIT PARAMETERS

j	a_j	k_j	\mathcal{G}_{j}	\mathcal{H}_{j}
2	0.6500	0	0.1023	20.0
3 (torso)	0.0000	0	-0.1750	20.0
4	-0.6500	1	0.0373	20.0
5	-1.8261	1	-0.1706	25.5

V. CASE STUDY: FIVE-DOF BIPED

A. Gait Selection

We consider a five-link biped with kinematic and dynamic parameters in Table I. The expressions for the matrices in (2) are not provided here but can be deduced from [26]. We design a gait following the approach in the Appendix. Thus, (20) can be rewritten as:

$$\theta_{i} = a_{i}\theta_{1} + k_{i}\pi + \mathcal{G}_{i}\sin(\mathcal{H}_{i}\theta_{1}), \quad j = 2, 3, 4, 5$$
 (44)

For $\theta_1^i = \pi/20$, a set of feasible gait parameters are listed in Table II. These parameters result in a gait with a stride length of 0.5371 m.

Remark 7: The stride length can be changed by simply changing the value of θ_1^i and recomputing the gait parameters using the algebraic relations in the Appendix.

Using (44) and the parameters in Table II, the VHCs in (29) can be expressed as:

$$\rho(q) = q_1 - \Phi(q_2) = 0, \quad \Phi: S^1 \to \mathcal{Q}^4$$

$$\Phi(q_2) = \begin{bmatrix} -0.3500q_2 + 0.1023\sin(20q_2) \\ -0.6500q_2 - 0.2773\sin(20q_2) \\ -0.6500q_2 + 0.2123\sin(20q_2) \\ -1.1761q_2 - 0.0373\sin(20q_2) - 0.1706\sin(25.5q_2) \end{bmatrix}$$

which satisfy the condition in Remark 4, and the condition in Remark 5 for $q_2 \in (-1.395, 1.395)$, which includes the range of operation of the passive joint $q_2 \in (-\pi/20, \pi/20)$. The gains of the continuous controller in (31) were chosen as $k_p = 450\,I_4$ and $k_d = 40\,I_4$, where $I_n \in R^{n \times n}$ is the identity matrix.

The desired orbit \mathcal{O}^* , defined by (34) and (35), can be specified by the independent choices of θ^i_1 and $\dot{\theta}^i_1$; for $\theta^i_1 = \pi/20$, we choose $\dot{\theta}^i_1 = -1.0891$ rad/s. This results in an average walking speed of 1.1554 m/s.

Remark 8: For a family of gaits, specified by $\hat{\theta}_1^i$ and its accompanying gait parameters, the walking speed can be changed by simply changing the value of $\hat{\theta}_1^i$, as long as $\hat{\theta}_1^i$ is greater than some minimum value - see Section III-D.

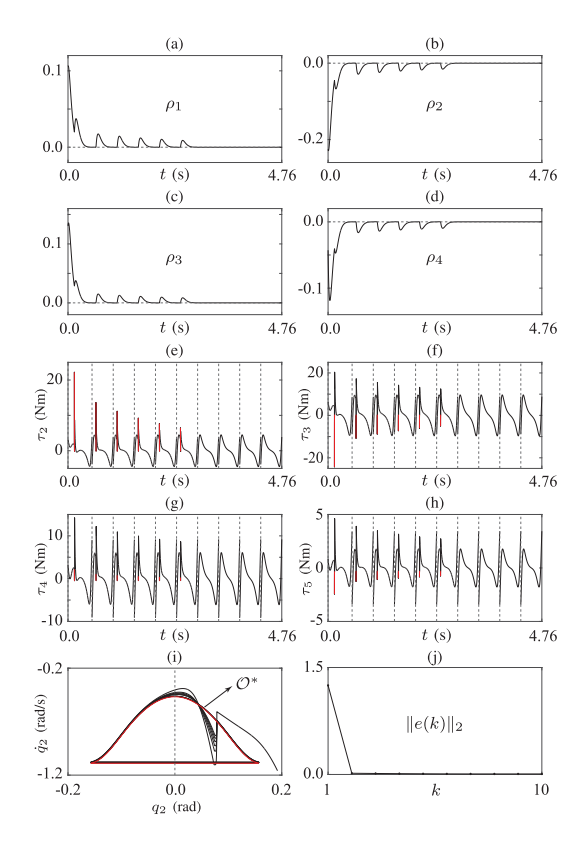
B. Stabilization of \mathcal{O}^*

We choose the following Poincaré section:

$$\Sigma = \{ x \in \mathcal{Q}^5 \times R^5 : q_2 = \pi/40, \dot{q}_2 < 0 \}$$
 (45)

on which the states are denoted by $z,z\in \mathcal{Q}^4\times R^5$, defined in (37). It was verified numerically that \mathcal{O}^* is transversal to Σ . The intersection of \mathcal{O}^* with Σ in (45) is the fixed point z^* of the map \mathbb{P} , and satisfies (39). The matrices $\mathcal{A}\in R^{9\times 9}$ and $\mathcal{B}\in R^{9\times 4}$ in (41) are computed numerically [3]; they are not provided here for brevity. The eigenvalues of \mathcal{A} do not all lie within the unit circle, but the pair $(\mathcal{A},\mathcal{B})$ is controllable. The gain matrix \mathcal{K} in (42), which asymptotically stabilizes \mathcal{O}^* , is obtained using LQR; the weighting matrices were

$$Q = \text{blockdiag} \begin{bmatrix} I_4 & 1.5I_5 \end{bmatrix}, \quad R = 2.5I_4$$



Orbital stabilization of an impact-free gait using the ICPM approach: (a)-(d) show the components of $\rho(q)$, (e)-(h) show the joint torques τ_i , j=2, 3, 4, 5, with impulsive torques shown in red, (i) shows the phase portrait of the passive coordinate q_2 , and (j) shows the norm of the error in states on the Poincaré section

Remark 9: The results in this section illustrate that gait design and control design for gait stabilization are decoupled.

C. Simulation Results

The initial configuration is taken as $x(0) = [q^T(0) \ \dot{q}^T(0)]^T$

$$q(0) = \begin{bmatrix} -0.027 & -0.172 & 2.011 & -0.055 & 0.192 \end{bmatrix}^T$$

$$q(0) = \begin{bmatrix} -0.027 & -0.172 & 2.011 & -0.055 & 0.192 \end{bmatrix}^T$$

$$\dot{q}(0) = \begin{bmatrix} 2.469 & -5.121 & 5.436 & -3.169 & -1.159 \end{bmatrix}^T$$

which does not lie on \mathcal{O}^* . Simulation results of the ICPM approach to gait stabilization are shown in Fig. 6 for 10 steps, which corresponds to a duration of approx. 4.76 s. The impulsive control in (42) is realized in the simulations using high-gain feedback u_{hg} in (43) with $\Lambda = I_4$, $\mu = 0.0005$, and $\epsilon = 0.0001$; the components of $\rho(q)$ are plotted in Fig. 6(a)-(d); these plots demonstrate convergence of system trajectories to the constraint manifold \mathcal{C} . The joint torques τ_j , j=2,3,4,5 , are shown in Fig. 6(e)–(h), with $u_{\rm hg}$ shown in red. Since $u_{\rm hg}$ causes system trajectories to leave C, the magnitude of u_c is large immediately after $u_{\rm hg}$ terminates. It can be seen that impulsive torques are not applied for k > 6 as the system trajectories are sufficiently close to \mathcal{O}^* . The instants of leg interchange are shown using dotted lines; the torques on either side of a dotted line therefore do not correspond to the same physical motor. The phase portrait of the passive coordinate q_2 is shown in Fig. 6(i). The desired orbit \mathcal{O}^* is shown in red; it is observed that system trajectories asymptotically converge to \mathcal{O}^* . Finally, $||e(k)||_2$, $k = 1, 2, \dots, 10$, is plotted in Fig. 6(j), which demonstrates asymptotic convergence of the states z(k) on Σ to z^* . For no slip of the stance foot, the minimum coefficient of friction required was found to be ≈ 0.57 .

Remark 10: Our approach does not explicitly constrain the joint torques or the required coefficient of friction, but stride length and walking speed can be chosen to satisfy these constraints. In this regard, FROST [29] provides a framework for the design and control of bipedal locomotion subject to explicit constraints.

The controller based on the ICPM approach effectively mitigates the foot-ground impact forces with each step. Both the impact force from the ground and impulsive control input converge to zero as the trajectory approaches \mathcal{O}^* .

Remark 11: The biped gait was simulated over a terrain with discrete changes in the height of the ground. An increase (decrease) in the height of the ground can be accommodated by a commensurate increase (decrease) in the parameters \mathcal{H}_j during the swing phase. Robustness of the gait and control designs to uneven terrain requires additional investigation.

Two animations are uploaded as supplementary material. The first animation shows stabilization of the impact-free gait that is simulated - see Fig. 6. The second animation compares this gait with another gait that has a longer stride length but equal walking speed.

VI. CONCLUSION

A method for designing and stabilizing impact-free gaits is presented for point-foot planar bipeds. The method allows gait design and gait stabilization to be treated as separate problems that can be addressed independently. The approach to gait design is computationally inexpensive, guarantees the existence of a solution, and allows the stride length and walking speed to be chosen independently while ensuring that impact forces are not generated at the time of swing foot touchdown. Virtual holonomic constraints are enforced by a continuous controller; this confines the system trajectories to a constraint manifold that contains a family of impact-free gaits. To stabilize a desired gait on the constraint manifold, the impulse controlled Poincaré map approach is used wherein impulsive inputs are applied intermittently. As the system trajectory converges to the desired impact-free gait, the magnitude of the impulsive inputs converge to zero. The procedure for gait design and stabilization is illustrated with the help of a five-link biped example. Future work will focus on gait design for inclined surfaces, robustness of the gait and control designs, experimental verification, as well as extension to non-planar biped robots.

APPENDIX EXISTENCE OF GAITS FOR n-DOF BIPEDS

We present a constructive proof that gaits defined by the trajectories in (20) can always be found for bipeds with $n \geq 5$. We assume the following form for $f_i^o(\theta_1)$:

$$f_i^o(\theta_1) = \mathcal{G}_i \sin(\mathcal{H}_i \theta_1) \tag{46}$$

where $\mathcal{G}_j, \mathcal{H}_j \in R, j = 2, 3, \dots, n$, are constants. This results in 4(n-1) parameters which, for a feasible choice of $\theta_1^i \in$ $(0, \pi/2)$, must satisfy the n+1 conditions in (23a), (24), (26) and (28). It is assumed that $\dot{\theta}_1^i \neq 0$, which is a necessary condition for the biped to take a step.

Parameters for j = n:

 $\overline{\text{Using } j = 1 \text{ in (23a)}}$ and (26), and substituting the expressions for θ_n and $\dot{\theta}_n$ from (20) and (21), we get:

$$(a_n + 1)\theta_1^i + \mathcal{G}_n \sin(\mathcal{H}_n \theta_1^i) + (k_n - 1)\pi = 0$$
 (47)

$$(a_n - 1) + \mathcal{G}_n \mathcal{H}_n \cos(\mathcal{H}_n \theta_1^i) = 0 \tag{48}$$

We choose $k_n = 1$ and \mathcal{H}_n arbitrarily; the other two parameters a_n and \mathcal{G}_n can then be obtained from solving:

$$\begin{bmatrix} \theta_1^i & \sin(\mathcal{H}_n \theta_1^i) \\ 1 & \mathcal{H}_n \cos(\mathcal{H}_n \theta_1^i) \end{bmatrix} \begin{bmatrix} a_n \\ \mathcal{G}_n \end{bmatrix} = \begin{bmatrix} -\theta_1^i \\ 1 \end{bmatrix}$$
(49)

which has a unique solution as long as the matrix on the LHS of (49) is nonsingular, i.e., as long as $\tan(\mathcal{H}_n\theta_1^i) \neq \mathcal{H}_n\theta_1^i$.

Parameters for $j = 2, 3, ..., (n-1), j \neq (n+1)/2$: For each j = 2, 3, ..., (n-1)/2 in (23a) and (26) we

For each $j=2,3,\ldots,(n-1)/2$ in (23a) and (26), we substitute the joint trajectories from (20) and (21) to get:

$$(a_j + a_{n-j+1})\theta_1^i + (k_j + k_{n-j+1} - 1)\pi + \mathcal{G}_j \sin(\mathcal{H}_j \theta_1^i) + \mathcal{G}_{n-j+1} \sin(\mathcal{H}_{n-j+1} \theta_1^i) = 0$$
 (50)

$$(a_j - a_{n-j+1}) + \mathcal{G}_j \mathcal{H}_j \cos(\mathcal{H}_j \theta_1^i)$$

$$-\mathcal{G}_{n-j+1}\mathcal{H}_{n-j+1}\cos(\mathcal{H}_{n-j+1}\theta_1^i) = 0 \tag{51}$$

We choose $k_j = 0$, $k_{n-j+1} = 1$, and $\mathcal{H}_j = \mathcal{H}_{n-j+1} = \pi/\theta_1^i$ for j = 2, 3, ..., (n-1)/2; then (50) and (51) reduce to:

$$(a_j + a_{n-j+1})\theta_1^i = 0 \implies a_{n-j+1} = -a_j$$
 (52)

$$(a_{i} - a_{n-i+1}) - (\mathcal{G}_{i} - \mathcal{G}_{n-i+1})\pi/\theta_{1}^{i} = 0$$
 (53)

Using (52) in (53) gives

$$\mathcal{G}_{n-j+1} = \mathcal{G}_j - 2a_j\theta_1^i/\pi \tag{54}$$

With the parameter choices so far, (28) may be rewritten as:

$$\ell_1 \sin \theta_1^i + \sum_{j=2}^{(n-1)/2} \ell_j \sin(a_j \theta_1^i) \left(a_j - \mathcal{G}_j \pi / \theta_1^i \right) = 0 \quad (55)$$

which permits a nontrivial solution only when $n \ge 5$. We arbitrarily choose the parameter $a_j \ne 0$ and choose any combination of \mathcal{G}_j 's to satisfy the above equation.

With a_j , \mathcal{G}_j now chosen, substitution of their values into (52) and (54) gives the values of a_{n-j+1} and \mathcal{G}_{n-j+1} .

Parameters for torso j = (n+1)/2:

We have from (24), (20) and (46):

$$a_i \theta_1^i + k_j \pi + \mathcal{G}_i \sin(\mathcal{H}_i \theta_1^i) = 0 \tag{56}$$

We choose $k_j = 0$ and $\mathcal{H}_j = \pi/\theta_1^i$. The above equation then requires that $a_j = 0$; then \mathcal{G}_j can be chosen arbitrarily.

The above approach guarantees that a gait can be found when $n \geq 5$, and provides significant flexibility in choice of gait parameters. Since the parameters are only subject to algebraic constraints, their computation does not adversely scale with the value of n.

REFERENCES

- A. Shiriaev, J. Perram, and C. C.-d. Wit, "Constructive tool for orbital stabilization of underactuated nonlinear systems: Virtual constraints approach," *IEEE Trans. Autom. Control*, vol. 50, no. 8, pp. 1164–1176, Aug. 2005.
- [2] M. Maggiore and L. Consolini, "Virtual holonomic constraints for Euler-Lagrange systems," *IEEE Trans. Autom. Control*, vol. 58, no. 4, pp. 1001–1008, Apr. 2013.
- [3] N. Kant and R. Mukherjee, "Orbital stabilization of underactuated systems using virtual holonomic constraints and impulse controlled Poincaré maps," Syst. Control Lett., vol. 146, 2020, Art. no. 104813.
- [4] A. Mohammadi, M. Maggiore, and L. Consolini, "Dynamic virtual holonomic constraints for stabilization of closed orbits in underactuated mechanical systems," *Automatica*, vol. 94, pp. 112–124, 2018.
- [5] E. Westervelt, J. Grizzle, and D. Koditschek, "Hybrid zero dynamics of planar biped walkers," *IEEE Trans. Autom. Control*, vol. 48, no. 1, pp. 42–56, Jan. 2003.
- [6] C. Chevallereau, J. W. Grizzle, and C.-L. Shih, "Asymptotically stable walking of a five-link underactuated 3-D bipedal robot," *IEEE Trans. Robot.*, vol. 25, no. 1, pp. 37–50, Feb. 2009.

- [7] E. R. Westervelt et al., Feedback Control of Dynamic Bipedal Robot Locomotion. Boca Raton, FL, USA: CRC Press, Oct. 2018.
- [8] F. Plestan, J. W. Grizzle, E. R. Westervelt, and G. Abba, "Stable walking of a 7-DOF biped robot," *IEEE Trans. Robot. Automat.*, vol. 19, no. 4, pp. 653–668, Aug. 2003.
- [9] A. Hereid, C. M. Hubicki, E. A. Cousineau, and A. D. Ames, "Dynamic humanoid locomotion: A scalable formulation for HZD gait optimization," *IEEE Trans. Robot.*, vol. 34, no. 2, pp. 370–387, Apr. 2018.
- [10] L. B. Freidovich, A. S. Shiriaev, and I. R. Manchester, "Stability analysis and control design for an underactuated walking robot via computation of a transverse linearization," *IFAC Proc. Volumes*, vol. 41, no. 2, pp. 10166–10171, 2008.
- [11] R. D. Gregg, T. Bretl, and M. W. Spong, "Asymptotically stable gait primitives for planning dynamic bipedal locomotion in three dimensions," in *Proc. IEEE Int. Conf. Robot. Automat.*, 2010, pp. 1695–1702.
- [12] J. Grizzle, G. Abba, and F. Plestan, "Asymptotically stable walking for biped robots: Analysis via systems with impulse effects," *IEEE Trans. Autom. Control*, vol. 46, no. 1, pp. 51–64, Jan. 2001.
- [13] E. Vukovich, "Virtual constraint generation for stable acrobot gaits," M.S. thesis, University of Toronto, Toronto, ON, Canada, 2020.
- [14] A. D. Ames, K. Galloway, K. Sreenath, and J. W. Grizzle, "Rapidly exponentially stabilizing control Lyapunov functions and hybrid zero dynamics," *IEEE Trans. Autom. Control*, vol. 59, no. 4, pp. 876–891, Apr. 2014.
- [15] F. Mathis, R. Jafari, and R. Mukherjee, "Impulsive actuation in robot manipulators: Experimental verification of pendubot swing-up," *IEEE/ASME Trans. Mechatronics*, vol. 19, no. 4, pp. 1469–1474, Aug. 2014.
- [16] R. Jafari, F. B. Mathis, R. Mukherjee, and H. Khalil, "Enlarging the region of attraction of equilibria of underactuated systems using impulsive inputs," *IEEE Trans. Control Syst. Technol.*, vol. 24, no. 1, pp. 334–340, Jan. 2016.
- [17] N. Kant, R. Mukherjee, D. Chowdhury, and H. K. Khalil, "Estimation of the region of attraction of underactuated systems and its enlargement using impulsive inputs," *IEEE Trans. Robot.*, vol. 35, no. 3, pp. 618–632, Jun. 2019.
- [18] N. Kant, R. Mukherjee, and H. K. Khalil, "Stabilization of energy level sets of underactuated mechanical systems exploiting impulsive braking," *Nonlinear Dyn.*, vol. 106, no. 1, pp. 279–293, 2021.
- [19] L. L. Flynn, R. Jafari, and R. Mukherjee, "Active synthetic-wheel biped with torso," *IEEE Trans. Robot.*, vol. 26, no. 5, pp. 816–826, Oct. 2010.
- [20] T. Albahkali, R. Mukherjee, and T. Das, "Swing-up control of the pendubot: An impulse–momentum approach," *IEEE Trans. Robot.*, vol. 25, no. 4, pp. 975–982, Aug. 2009.
- [21] N. Kant and R. Mukherjee, "Impulsive dynamics and control of the inertia-wheel pendulum," *IEEE Robot. Automat. Lett.*, vol. 3, no. 4, pp. 3208–3215, Oct. 2018.
- [22] A. Khandelwal, N. Kant, and R. Mukherjee, "Nonprehensile manipulation of a stick using impulsive forces," *Nonlinear Dyn.*, vol. 111, pp. 113–127, 2023.
- [23] N. Kant and R. Mukherjee, "Juggling a devil-stick: Hybrid orbit stabilization using the impulse controlled Poincaré map," *IEEE Contr. Syst. Lett.*, vol. 6, pp. 1304–1309, 2022.
- [24] Y. Hurmuzlu and D. B. Marghitu, "Rigid body collisions of planar kinematic chains with multiple contact points," *Int. J. Robot. Res.*, vol. 13, no. 1, pp. 82–92, 1994.
- [25] J. W. Grizzle and C. Chevallereau, "Virtual constraints and hybrid zero dynamics for realizing underactuated bipedal locomotion," in *Humanoid Robotics: A Reference*, A. Goswami and P. Vadakkepat, Eds. Dordrecht, The Netherlands: Springer, 2019, pp. 1045–1075.
- [26] R. Jafari, L. L. Flynn, A. Hellum, and R. Mukherjee, "Energy-conserving gaits for point-foot planar bipeds: A Five-DOF case study," in *Proc. ASME Dyn. Syst. Control Conf.*, Palo Alto, CA, 2013.
- [27] C. Byrnes and A. Isidori, "Asymptotic stabilization of minimum phase nonlinear systems," *IEEE Trans. Autom. Control*, vol. 36, no. 10, pp. 1122–1137, Oct. 1991.
- [28] H. Khalil, Nonlinear Systems. Hoboken, NJ, USA: Prentice Hall, 2002.
- [29] A. Hereid and A. D. Ames, "FROST*: Fast robot optimization and simulation toolkit," in *Proc. IEEE/RSJ Int. Conf. Intell. Robots Syst.*, 2017, pp. 719–726.